Conformational dynamics and role of the acidic pocket in ASIC pH-dependent gating

Sabrina Vullo[a,1], Gaetano Bonifacio[a,1], Sophie Roy[a], Niklaus Johner[b,c], Simon Bernèche[b,c], and Stephan Kellenberger[a,2]

[a]Department of Pharmacology and Toxicology, Faculty of Biology and Medicine, University of Lausanne, 1011 Lausanne, Switzerland; [b]SIB (Swiss Institute of Bioinformatics), Biozentrum, University of Basel, 4056 Basel, Switzerland; and [c]Biozentrum, University of Basel, 4056 Basel, Switzerland

Edited by William A. Catterall, University of Washington School of Medicine, Seattle, WA, and approved February 22, 2017 (received for review December 14, 2016)

Acid-sensing ion channels (ASICs) are proton-activated Na^+ channels expressed in the nervous system, where they are involved in learning, fear behaviors, neurodegeneration, and pain sensation. In this work, we study the role in pH sensing of two regions of the ectodomain enriched in acidic residues: the acidic pocket, which faces the outside of the protein and is the binding site of several animal toxins, and the palm, a central channel domain. Using voltage clamp fluorometry, we find that the acidic pocket undergoes conformational changes during both activation and desensitization. Concurrently, we find that, although proton sensing in the acidic pocket is not required for channel function, it does contribute to both activation and desensitization. Furthermore, protonation-mimicking mutations of acidic residues in the palm induce a dramatic acceleration of desensitization followed by the appearance of a sustained current. In summary, this work describes the roles of potential pH sensors in two extracellular domains, and it proposes a model of acidification-induced conformational changes occurring in the acidic pocket of ASIC1a.

acid-sensing ion channel | conformational changes | voltage clamp fluorometry | pH sensing | kinetic model

Acid-sensing ion channels (ASICs) are Na^+-permeable channels (1) that participate in neuronal signaling under conditions involving pH changes, such as neuronal activity, ischemia, and inflammation. ASICs are involved in fear behaviors, learning, neurodegeneration after ischemic stroke, and pain sensation (2, 3). Functional ASICs are composed of three identical or homologous subunits (4, 5).

These channels respond to extracellular acidification with a transient current, because, after opening, they rapidly enter a nonconducting, so-called "desensitized" functional state. Crystal structures of chicken ASIC1 (~90% sequence homology to human ASIC1a) reveal presumably desensitized (5, 6) and toxin-opened conformations (7–9). Single ASIC subunits have a shape similar to that of a hand holding a small ball (5), and thus their domains have been named accordingly (Fig. 1*A*). The palm domain forms the internal scaffold of the channel along the central vertical axis. The thumb and the finger point toward the exterior of the channel and enclose, together with the β-ball, the "acidic pocket" (AcP), a region containing many acidic residues (Fig. 1*A*) (5).

Due to the presence of many acidic residues, the AcP was initially proposed as a pH sensor of ASICs (5). Although mutation of AcP Glu and Asp residues shifts the pH dependence of ASIC activation to more acidic values (5, 10–12), H^+-sensing residues have also been identified outside the AcP (10, 12, 13), indicating that the AcP is not the only extracellular pH-sensing domain. Its importance is, however, underlined by the fact that it constitutes the binding site of several ASIC-specific toxins (7, 14).

In the present study, we asked whether acid sensing in the AcP and the palm is required for ASIC activation and whether the timing of conformational changes in the AcP is compatible with a role in activation. We show that combined, conservative mutation of potential pH-sensing residues in the AcP changes the pH dependences, but still allows ASIC opening and desensitization. Analogous mutations in the palm accelerated desensitization and led to the appearance of a secondary, sustained current. Voltage clamp fluorometry (VCF) analysis indicates the occurrence of rapid and slow conformational changes in the AcP, compatible with a role in both activation and desensitization, and allows us to propose a model of conformational changes in this domain.

Results

Acidic Residues in the Acidic Pocket Are Not Required for ASIC Activation. To determine the importance of pH sensing in the AcP for ASIC1a function, we combined neutralization mutations of all Asp, Glu, and His residues of the AcP to Asn or Gln (Fig. 1 *A* and *B*). When all of the protonable residues of the AcP were mutated, these channels, expressed in *Xenopus* oocytes, still produced transient currents upon extracellular acidification. Some mutants displayed up to twofold accelerated kinetics of current decay (Fig. S1*A*), in accordance with previous studies that described altered current kinetics of AcP mutants (15, 16). Some mutants showed a sustained current, which was, however, small in all mutants except AcP16b (Fig. S1*B*), indicating that desensitization is, in most mutants, complete at the end of an acidification.

The pH of half-maximal activation (pH50) was generally shifted by ~0.5 pH units to more acidic values compared with WT (green symbols and bars in Fig. 1 *D* and *E*). The Hill coefficient, a measure of the steepness of the pH-current relationship and of the cooperativity of the process, decreased from ~3 in WT to ~1.5 in most channels containing more than seven AcP mutations (gray

Significance

Many physiological processes are regulated by pH. The acid-sensing ion channels (ASICs) are neuronal pH sensors involved in learning, fear behavior, neurodegeneration after ischemic stroke, and pain sensation. The mechanism by which acidic pH activates ASICs is still poorly understood. We show here that the "acidic pocket," the binding site of several toxins, is not essential for channel function but has, rather, a modulatory role. Furthermore, we describe the structural rearrangements occurring in this domain during ASIC activity, and highlight the importance of the "palm" domain in channel opening and current decay. In this study, we provide insights on the molecular mechanisms controlling ASIC activity together with a rational basis for the development of ASIC-targeting drugs.

Author contributions: G.B. and S.K. designed research; S.V., G.B., S.R., and N.J. performed research; S.V., G.B., S.R., N.J., S.B., and S.K. analyzed data; and S.V., N.J., and S.K. wrote the paper.

The authors declare no conflict of interest.

This article is a PNAS Direct Submission.

[1]S.V. and G.B. contributed equally to this work.

[2]To whom correspondence should be addressed. Email: stephan.kellenberger@unil.ch.

This article contains supporting information online at www.pnas.org/lookup/suppl/doi:10.1073/pnas.1620560114/-/DCSupplemental.

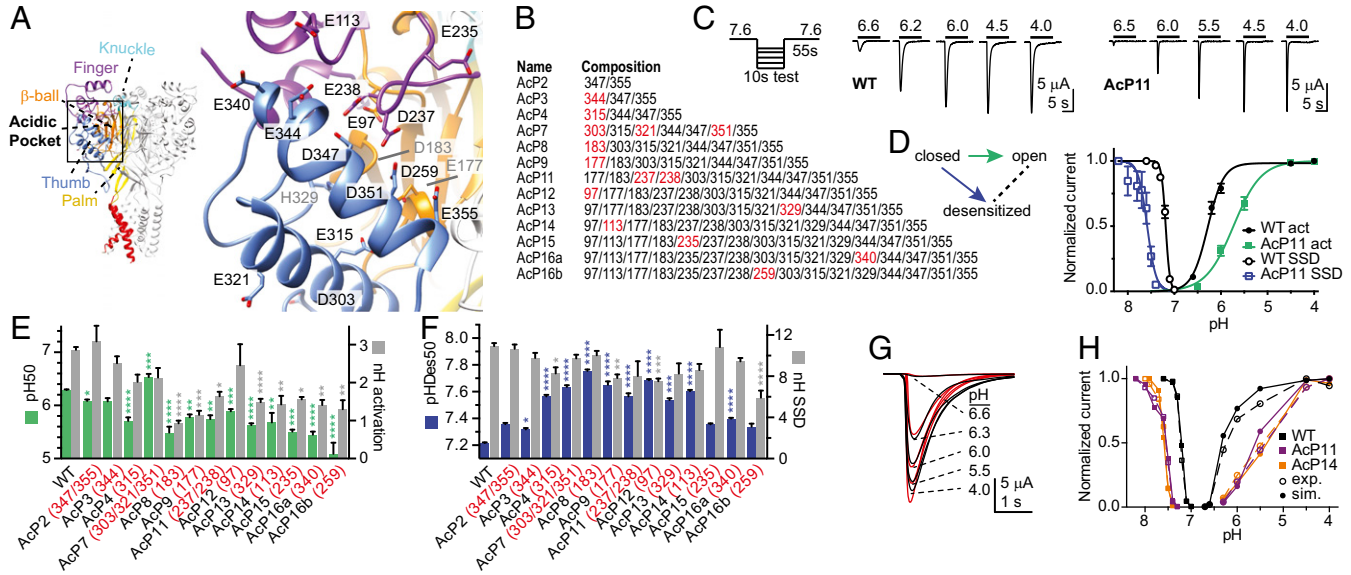

Fig. 1. Combined mutation of AcP residues preserves almost normal ASIC1a function. (*A*) Structural image, showing a human ASIC1a model based on the chicken ASIC1 structure (8). (*Left*) Trimer structure. Individual domains of one subunit are colored and labeled. (*Right*) Close-up view of the AcP formed by the thumb, the finger, and the β-ball. The residues that were mutated are indicated. (*B*) Mutant composition. Each number in the right column represents a neutralization mutation, Glu to Gln, Asp to Asn, and His to Asn. The new mutations from one construct to another are marked in red. (*C*) Representative current traces of WT and the mutant AcP11. The pH protocol is schematically indicated on the left. (*D*) The pH dependence of activation and SSD of WT and AcP11 ($n = 4–6$). Normalized current amplitudes are plotted as a function of stimulation pH for activation (filled symbols) and as a function of the conditioning pH for SSD (open symbols). The solid lines represent fits to the Hill equation (*SI Materials and Methods*). The kinetic scheme of ASIC functional states is shown, emphasizing, with a green arrow, the activation, and, with a blue arrow, the SSD transition. (*E*) The pH dependence of activation, plotting pH of half-maximal activation (pH50) values as green bars (left axis) and the Hill coefficient (nH) in gray (right axis). The conditioning pH in these experiments was 7.6 to 8.0, depending on the mutant, to ensure stable recordings without occurrence of SSD. For each mutant, the numbers in red indicate the residues mutated in addition to the mutations already present in the preceding mutant; $n = 4–125$. (*F*) The pH dependence of SSD, showing pH of half-maximal SSD, pHDes50 values as blue bars, and nH values of SSD in gray; $n = 5–56$. (*G*) Experimental current traces (black) of an activation curve of ASIC1a WT and corresponding traces generated by the 32-state model (red; *SI Materials and Methods*). (*H*) Activation and SSD curves of WT, AcP11, and AcP14 generated experimentally (filled symbols) or by the 32-state model (open symbols). (*$P < 0.05$; **$P < 0.01$; ***$P < 0.001$; ****$P < 0.0001$; different from WT.)

bars in Fig. 1*E*). The pH dependence of steady-state desensitization (SSD), the direct transition from the closed to the desensitized state (blue arrow in the scheme of Fig. 1*D*), was determined by exposing oocytes to a series of conditioning test pH solutions for 55 s, each followed by a short application of an acidic pH solution. The pH dependence of SSD was shifted to more alkaline values by the combination of AcP mutations (blue symbols and bars in Fig. 1 *D* and *F*), although the values are less alkaline for constructs containing >14 neutralization mutations.

As shown above, neutralization mutations of protonable residues in the AcP induced the following functional changes: (*i*) They shift the pH50 of activation to more acidic values; (*ii*) they shift the pH50 of SSD to more alkaline values; and (*iii*) they decrease the Hill coefficient of activation, but not of SSD. Neutralization mutations of Asp and Glu, mimicking protonated acidic residues, correspond to gain of function mutations, which are expected to lead to an alkaline shift in pH dependence as observed for neutralization mutations of key proton-sensing residues in the K^+ channel KcsA (17). Although our mutagenesis approach does not indicate whether a mutated residue is a pH sensor or has other roles in conformational transitions, it is very likely that at least some of these residues are pH sensors. Because the observed effects of AcP mutations appear to be complex, we use kinetic models to illustrate how these mutations may affect pH dependence. Consider a four-state model as depicted in Fig. S1*C*, corresponding to a system with two protonation sites, either of which can be protonated or not. A neutralization mutation will correspond to having one of the sites always protonated, reducing the problem to a two-state model. We show that, if protonation of both sites is required for the transition to the state of interest (e.g., the open state), then a neutralization mutation will always lead to an increase in pH50 accompanied by a decrease of the Hill coefficient (*SI Materials and Methods* and Fig. S1*D*). However, if protonation of only one of the sites is required, then mutation of the other one can lead to both an increase or a decrease in pH50 and an increase or a decrease in the Hill coefficient (Fig. S1 *D* and *E* and *SI Materials and Methods*). The observed effects of AcP mutations therefore suggest a nonessential role of this domain in activation. To test this hypothesis, we built a kinetic model of ASIC comprising three sets of protonation sites: (*i*) sites in the AcP, (*ii*) other sites responsible for desensitization, and (*iii*) sites leading to activation (Fig. S1*F* and *SI Materials and Methods*). The model was fitted to traces of complete activation and SSD curves of ASIC1a WT and the mutants AcP11 and AcP14. The model reproduced the experimental data reasonably well if protonation of the AcP was considered accessory for activation, regardless of whether the same protonation events in the AcP were modeled as required or were accessory for desensitization (Fig. 1 *G* and *H* and Fig. S1*F*), but not if they were considered essential for activation. The parameters of the fitted models indicated that protonation of the AcP shows a negative cooperativity with protonation of activation sites, and a positive cooperativity with protonation of desensitization sites. The modeling suggests, therefore, that protonation-mimicking mutations of the AcP induced an acidic shift in activation pH dependence due to the negative cooperativity between these two types of protonation.

Combined Mutations of Potential pH Sensors in the Palm Accelerate Desensitization and Give Rise to a Nondesensitizing Current. To assess the role of pH sensing in the palm, we combined mutations

of the six acidic residues of the lower and middle palm (palm core, "PaC," bold in Fig. 2*A*), and subsequently, in addition, the two nearby β-ball residues D212 and E254 (Fig. 2 *A* and *B*). The most striking feature of these combined mutants is the appearance of a sustained current component and, with increasing number of mutations, a complete disappearance of the transient current (Fig. 2*C* and Fig. S2*A*). The disappearance of the peak current could be due to either loss of channel activation or very fast desensitization; to distinguish between these two possibilities, we measured the mutant channels at a lower temperature, which is known to strongly slow down desensitization but not activation (18). We uncovered a peak current in PaC6, and observed a strong increase of the PaC4 peak current amplitude relative to that of the sustained current (Fig. 2*D* and Fig. S2*B*). This demonstrates that the combined mutations such as PaC6 accelerate desensitization to an extent that the transient current disappears.

The slowly developing sustained current is only induced by cumulative palm mutations, as no single neutralization mutation of acidic residues of the palm, except for D78, induced any sustained currents (Fig. S2*C*). This sustained current is distinct from the transient current with regard to several properties. (*i*) In contrast to the WT peak current, the sustained current has almost completely lost its cation selectivity (Fig. S2 *D–G*; P_{Na}/P_K ratio of 9.8 ± 0.4, 5.2 ± 0.4, 2.5 ± 0.3 and 2.7 ± 0.9 for WT, PaC4 peak, PaC4, and PaC6 sustained current, respectively; n = 3–11, $P < 0.01$); (*ii*) it is not inhibited by the pore blocker amiloride (Fig. S2 *H* and *I*); and (*iii*) its pH dependence of activation is shifted by two pH units to more acidic values (Fig. 2*E*).

Additional mutation of the two acidic palm residues pointing toward the wrist, D78 and E421, or the wrist residue H73 (Fig. S2*J*) in PaC mutants did not further change the current properties in most cases (Fig. S2 *K–N*). In two of these mutants, a transient current was reconstituted. The pH dependence of the tested palm mutants correlated with the type of current—transient vs. sustained—and not with the number of mutations (Fig. 2*E* and Fig. S3*M*). This correlation, together with the different current properties, further confirms that these nondesensitizing currents are profoundly different types of openings, and may be related to sustained ASIC currents induced by some chemical compounds and lipids (19, 20).

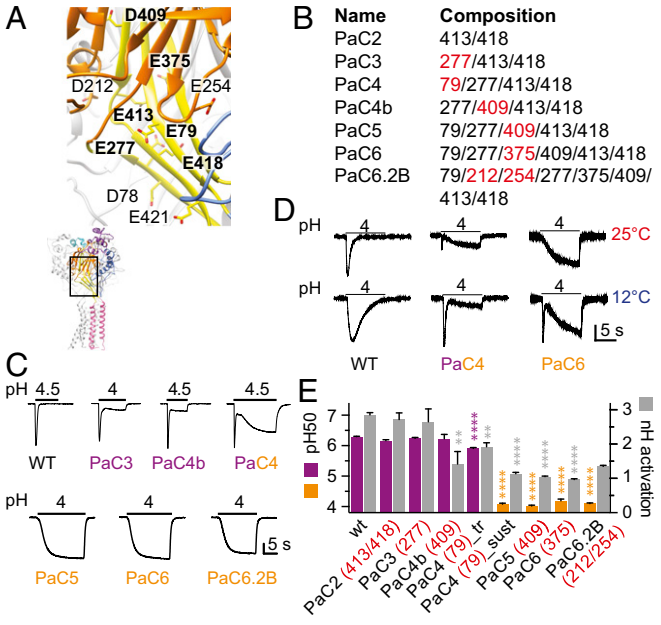

Fig. 2. Combined mutations of palm residues accelerate desensitization and induce a sustained current. (*A*) Structural image of the palm (yellow) and β-ball (orange) domains of one ASIC1a subunit, showing the acidic residues investigated here, with residues of the "palm core" (see *Results*) highlighted in bold. (*B*) Mutant composition. The new mutations from one construct to another (compared with the construct with lower number of mutations) are marked in red. B, β-ball; PaC, palm core. (*C*) Representative current traces of different palm mutants. The vertical bar corresponds to (in microamperes) 6 (WT), 3 (PaC3), 4 (Pa4b), 1 (PaC4), 1.25 (PaC5), 0.5 (PaC6), and 0.24 (PaC6.2B). (*D*) Representative current recordings of WT, PaC4, and PaC6 at the indicated temperatures. The vertical bar corresponds to (in microamperes) 4.6 (WT), 3.2 (PaC4), and 1 (PaC6). In *C* and *D*, the conditioning pH was 7.4. (*E*) The pH dependence of activation, pH50 values (colored bars), and nH of activation (gray bars); n = 5–128. The pH50 values of transient currents are shown in purple, and those of sustained currents are shown in orange. (*$P < 0.05$; **$P < 0.01$; ***$P < 0.001$; ****$P < 0.0001$; different from WT.)

Conformational Changes in the Acidic Pocket. By which mechanisms do the palm and the AcP influence ASIC function? The comparison of toxin-opened and desensitized ASIC structures showed evidence for a centripetal movement of the three lower palm domains during desensitization (7). Accessibility studies combined with molecular dynamics simulations suggested that this conformational change in the palm is transduced into closure of the pore (21).

To obtain information on possible conformational changes in the AcP during gating, we applied VCF, which employs simultaneous measurement of ionic currents and of the fluorescence intensity of fluorophores placed at specific sites of the channel (Fig. 3*A*). Attachment of the fluorophores AlexaFluor488 (Fig. 3*B*) or CF488A to engineered Cys residues at different positions of the AcP did not, in most mutants, lead to measurable fluorescence changes (ΔF) during channel activity (Table S1). Changes in fluorescence intensity of fluorophores are due to alterations in the environment and/or quenching by nearby amino acid residues. Trp is known as a strong fluorescence quencher (22). To allow the measurement of ΔF signals in this domain, we have paired engineered Cys residues as fluorophore docking positions with engineered Trp residues as quenchers across the AcP (Fig. 3*A* and Fig. S3*A*).

Cys/Trp double mutants of the AcP produced transient acid-induced currents, and various types of ΔF signals. The ΔF of several Cys/Trp mutants contained two components, an initial rapid negative or positive ΔF that was followed by a slower ΔF of the opposite polarity, as illustrated by current and ΔF traces of the mutant D237C/D347W (Fig. 3*C*, lower traces). To associate ΔF signals with functional transitions, we compared the kinetics of the ΔF and the current signals, measured as rise time (the time to pass from 10 to 90% of the full amplitude). We measured the pH 6-induced ΔF and currents from approximately the same oocyte surface by using a recording chamber in which the solution flows under the oocyte (Fig. 3*D* and *SI Materials and Methods*). The onset kinetics of the fast ΔF component of the mutants D347C/T236W, D237C/D347W, D351C/D237W, and E355C match the kinetics of current appearance (Fig. 3*E* and Fig. S3*B*; see Table S2 for a correlation analysis). These ΔF signals started 100 ms to 250 ms before the current (Fig. 3 *F* and *G*), strongly suggesting that the monitored movements in these mutants are correlated with channel opening. The second ΔF components and the ΔF signals of all other mutants were slower than current appearance (Fig. 3*E*), and the difference in delay was smaller or absent. The ΔF onset was, in most mutants, faster than the current decay (Fig. 3*H*), and only two mutants, K343C/T236W and D351C/F257W, showed ΔF onset kinetics correlated with current desensitization. The transitions occurring after channel opening may thus be associated with desensitization or with its preparation.

The pH dependence of the ΔF signals was, in most mutants, close to that of SSD, and was more alkaline than the pH dependence of current activation (Fig. 3*I*); hence these conformational

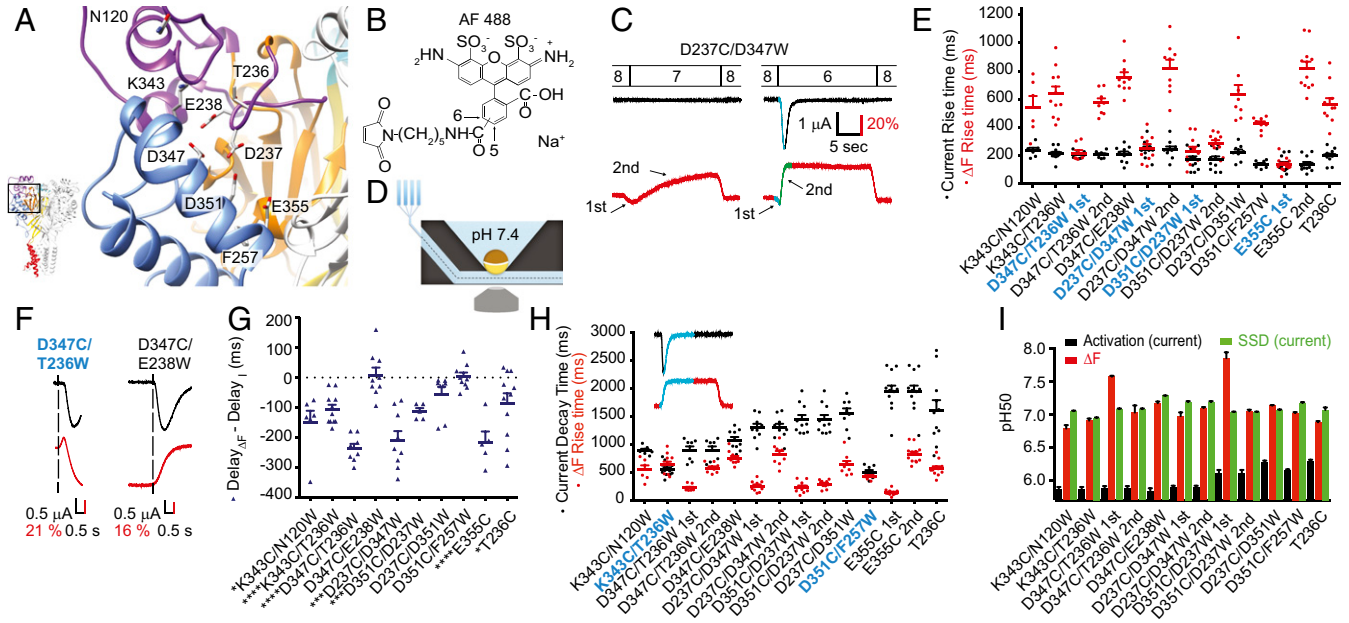

Fig. 3. Fluorescence changes in the AcP associated with channel opening and desensitization. (*A*) Close-up view of the AcP, showing the residues that were mutated to Cys (to dock fluorophores) and/or to the quenching residue Trp. (*B*) Structure of the fluorophore AlexaFluor488. (*C*) Representative current and Δ*F* traces at pH 7 and 6 of the mutant D237C/D347W, highlighting, in green and blue, the parts of the pH 6 traces used for kinetic analysis. Note that the Δ*F* trace has two components, as highlighted with the arrows. (*D*) Schematic view of the oocyte recording chamber used for measurements of current and Δ*F* kinetics (*SI Materials and Methods*). (*E*) Scatter graph comparing the rise time of the channel opening (black) and the Δ*F* onset (red) in response to acidification from the conditioning pH 7.4 to the stimulation pH 6 in paired experiments; $n = 6–12$. For mutants containing two Δ*F* components, the two are distinguished as first and second. Correlation between the Δ*F* and current signal is indicated by labeling in bold turquoise (see criteria in Table S2). (*F*) Representative current and Δ*F* traces showing (*Left*) a mutant in which the start of the Δ*F* signal precedes that of the current (D347C/T236W) and (*Right*) one in which the two signals start at the same time (D347C/E238W). The vertical dashed line indicates the beginning of the Δ*F*. (*G*) Scatter dot plot of the difference in the Δ*F* and current delay of appearance ($delay_{\Delta F} - delay_I$) measured at pH 6; $n = 5–11$. (*H*) Scatter graph comparing the current decay time (black) and the fluorescence rise time (red) in response to acidification from pH 7.4 to pH 6 in paired experiments; $n = 6–12$. Bold turquoise labels indicate correlation between Δ*F* onset and current decay kinetics (Table S2). (*Inset*) In blue, the parts of current and Δ*F* traces whose kinetics were compared. (*I*) The pH of half-maximal amplitude (pH50) for current (black columns) and fluorescence activation (red), and the pH of current SSD (green); $n = 4–16$.

changes could be part of channel desensitization. The Δ*F* signals sharing the kinetics of current appearance also showed such a shifted pH dependence, indicating that they occur at more alkaline pH than channel opening. This observation does not rule out their possible implication in channel opening, but it indicates that there must be other conformational changes required for activation, which have a lower pH50 than those occurring in the AcP and would therefore govern the pH50 of activation. This shift in pH dependence is reminiscent of the leftward shift in voltage dependence of Δ*F* versus currents in voltage-gated K^+ channels (23, 24).

Hypothesized Movements Based on VCF Observations. The proximity of a quenching group decreases the total fluorescence (*F*) of a fluorophore, but may generate an activity-induced Δ*F* if there is a change in distance between the fluorophore and the quenching group. The specific Δ*F* signals of the single Cys mutants used in the Cys/Trp pairs were of very small amplitude compared with the Δ*F* signal of related Cys/Trp pairs (Table S1), indicating that the Δ*F* observed in double mutants is due to the additional presence of the engineered Trp. Control experiments showed that the only endogenous Trp residue in the proximity of the palm, W233, did not affect these signals (compare Fig. S3*C* and Fig. 4*A*). A positive Δ*F* indicates, therefore, an increase in distance between the Trp residue and the Cys-attached fluorophore, whereas a negative Δ*F* indicates a decrease in this distance. These Δ*F* signals do not exactly reflect the distance changes between the Cys and Trp of a given pair, because the fluorophore has itself a diameter of 7 Å to 10 Å and is attached to the Cys residue by a linker (Fig. 3*B*), with an estimated distance between the docking site and the center of the fluorophore of 5 Å to 15 Å (from molecular dynamics trajectories, Corry research group, karri.anu.edu.au/handy/). This limitation has to be considered as a factor of imprecision in the following interpretation of the VCF data.

The nature of the Δ*F* signals of different Cys/Trp double mutants (Fig. 4*A*) is summarized in the ASIC structure (Fig. 4*B*) with dotted lines between the paired residues and with "+" indicating an increase, and "-" a decrease, in Δ*F*. The early, rapid Δ*F* signals suggest, therefore, a short-lived approach of D237 toward D347 and D351, and an increase of the T236–D347 distance, which occurs during or slightly before activation. The VCF analysis suggests that these movements are then followed by a decrease of the N120–K343 and T236–D347 distances, and by an increase of the D237–D347, D237–D351, and E238–D347 distances, and, with the time course of desensitization, an increase of the F257–D351 and a decrease of the K343–T236 distances.

We estimate that the higher amplitude of the slower Δ*F* components is due to a larger conformational change, because, in the Δ*F* signals composed of a rapid and a slow component, the Δ*F* of both components depends on the quenching by the engineered Trp, and rapid and slow signals were compared within the same Cys/Trp pair. Most likely, the conformational changes generating these Δ*F* signals are part of a continuous movement of the involved AcP domains. The initial, fast Δ*F* signals that are correlated with channel activation may represent a tilting of the finger loop that would bring D237 and E238, located at the lower end of the loop, closer to the α5 helix, and T236, which is higher up, farther away from the α5 helix (green arrows in Fig. 4*C*). The distance changes involving residues T236, D237, and E238 occurring

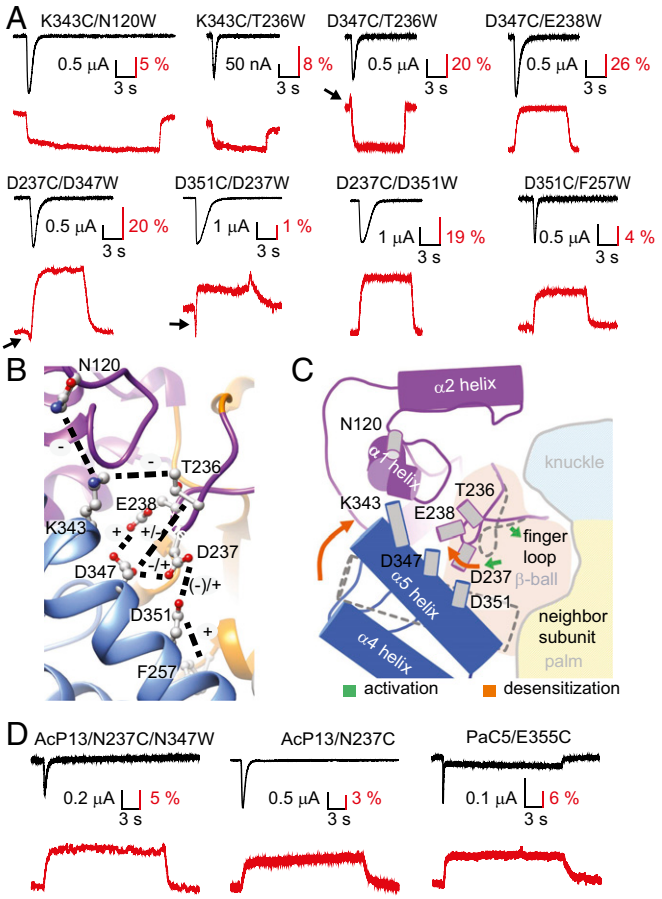

Fig. 4. Predicted conformational changes in the AcP. (*A*) Representative, paired current (black) and fluorescence (red) traces of double mutants in response to extracellular acidification to pH 6. Black arrows point to fast Δ*F* components. (*B*) View of the AcP with the mutated residues, indicating, by dashed black lines, the different Cys/Trp pairs. For each double mutant, the nature of the Δ*F* signal is indicated by "+" or "−" signs ("+" denotes increase in Δ*F*); for mutants with composite Δ*F* signal, the left sign represents the first component. (*C*) Scheme indicating the deduced conformational changes in the AcP during opening and steps preceding and correlated with desensitization, as discussed in the *Results*. The gray cylinders represent residues mutated for the VCF experiments. The dotted outlines of the finger loop and α5 thumb helix represent their hypothesized position in the closed state. Hypothesized conformational changes are illustrated by arrows, the green arrows standing for conformational changes occurring during activation, and the orange arrows standing for subsequent steps occurring before and during desensitization. (*D*) Representative current and Δ*F* traces of the mutants AcP13/N237C/N347C, AcP13/N237C, and PaC5/E355C. Note that not only the N237C/N347W pair, but also the single mutation N237C, induced measurable Δ*F* signals, indicating that, in the changed environment of the AcP13 mutant, the N237C Δ*F* did not depend on the presence of a nearby Trp residue and does not reflect a change in distance between the fluorophore and the Trp residue. The PaC5/E355C mutant showed, in approximately half of the experiments, a rapid transient and a sustained component and, in the other half, only a sustained current.

after activation are best explained by a movement of this finger loop toward the outside of the protein (right orange arrow in Fig. 4*C*). This movement may involve a partial rotation of the loop, thereby bringing T236 closer to K343 and D347, as well as moving D237 and E238 away from D347 and D351. The α5 helix likely undergoes a movement relative to the other domains that brings its outer end (K343) closer to the finger and its inner part (D351) farther away from the β-ball.

Δ*F* Signals in Mutants Containing Protonation-Impaired Domains. To determine whether conformational changes depend on protonation events in the AcP and the palm, we introduced a fluorophore/quencher pair in the AcP mutant AcP13, and the E355C mutation in the palm mutant PaC5, thus two mutants in which a large number of acidic residues have been neutralized. In both, AcP13/N237C/N347W and PaC5/E355C, the slow, but not the fast, Δ*F* component was present (Fig. 4*D* and Fig. S4). The absence of a fast Δ*F* component in these mutants may be due to a requirement of protonation of AcP or palm residues for the rapid Δ*F* signal. We cannot, however, exclude the possibility that this absence is due to a changed environment, especially for AcP13/N237C/N347W. The fact that the slower Δ*F* signal is still present in the combined mutants indicates that neither protonation of AcP nor palm residues is required for the slower conformational changes occurring in the AcP. E355C showed, as expected, faster current decay kinetics in the PaC5 background, and this acceleration was also reflected in the Δ*F* onset kinetics ($P < 0.0001$ and <0.05, respectively; Fig. S4*D*).

Discussion

We show, in this study, that the presence of protonable residues in the AcP and the palm is not essential for ASIC activation but plays other roles: In the AcP, acidic residues allow the fine-tuning of ASIC pH dependence, whereas, in the palm, they control the desensitization kinetics and prevent the appearance of a sustained current. Our VCF analysis provides evidence of conformational changes in the AcP correlated to activation and desensitization, and proposes a likely sequence of conformational changes in the AcP upon extracellular acidification.

The observed acceleration of the desensitization kinetics in palm mutants was much stronger than kinetic changes of palm mutants investigated in previous studies (10, 21) and led to the disappearance of the transient current at room temperature. The fact that acceleration was induced by mutations that mimic protonated side chains suggests that protonation events in the palm lead to desensitization.

The AcP is the binding site of the two gating modifier toxins PcTx1 and Mambalgin (7, 9, 25–27). Nonconservative mutations in the AcP of ASICs have induced strong changes in the pH dependence (11, 28), whereas conservative mutations of Asp and Glu residues induced modest (5, 12) or no changes in activation pH dependence (10). The acidic residues E344, D347, D351, and E355 of the thumb α5 helix that are at the center of the interaction with the finger loop are better conserved between ASIC1a and ASIC2 (three of four) than between ASIC1a and ASIC3 (one of four), whose pH dependence is close to that of ASIC1a. These differences appear not to affect the conformational changes in the AcP, because at least the slow Δ*F* signals were still present after neutralization of many AcP residues (Fig. 4*D*). For ASIC2, it was shown that regions outside the AcP, mostly the first ∼90 residues after the TM1, are critical for channel function (29, 30). These observations are consistent with an important regulatory, but not essential, role of the AcP in ASIC activation. The AcP also controls the kinetics and pH dependence of desensitization (15, 16, 27), a role that is underlined here by the slow Δ*F* signals, which may reflect conformational changes leading to desensitization. In ENaC, the AcP may also have a regulatory role, because it was shown to contain a binding site for Na^+ involved in channel inhibition (31).

Experimental evidence for conformational changes in the AcP was recently provided by luminescence resonance energy transfer (LRET) measurements showing that the distance between residues of the thumb and the finger is decreased in the desensitized compared with the closed state (28). We describe here the time course of this closing movement and suggest that it concerns, rather, the external end of the AcP, which opens on its inner side. Such a movement of the inner part of the AcP is supported by the recent observation that formation of a disulfide bond between the thumb residue E355C and R175C of the palm locks

the channel in the closed state (32). The slower conformational changes in the AcP do not depend on protonation events in the AcP or the palm, indicating that these conformational changes in the AcP are induced by protonation events occurring outside the AcP or the palm. Protonation of AcP residues, or binding of ligands to the AcP, may influence the kinetics and possibly the amplitude of these conformational changes and thereby modulate ASIC function.

Our observation of large ΔF signals occurring between opening and desensitization, suggesting conformational changes in the AcP, contradicts the findings with crystal structures of ASIC1, which show an almost identical conformation of the AcP in toxin-opened and desensitized channels (7). It is possible that the toxin-opened ASIC conformation studied in crystal structures is different from the H^+-opened conformation. Evidence for important conformational changes during ASIC desensitization comes from the observation that ASIC currents show a strong temperature dependence of desensitization. In contrast, the temperature dependence of activation is much weaker (18). These observations are consistent with the small-amplitude ΔF signals correlated to activation and the large-amplitude ΔF signals correlated to later events. The above-mentioned LRET experiments (28) and a recent Cys accessibility study (15) also suggest conformational changes in the AcP upon acidification. To affect channel activity, conformational changes in the AcP need to change the conformation of the ASIC pore. The downward movement of the internal end of the α5 helix during desensitization would likely be transmitted to the pore via the β-turn structure that is part of a palm−thumb loop and interacts with the external end of the transmembrane domain, or via the palm.

Materials and Methods

WT and mutant human ASIC1a were expressed in *Xenopus laevis* oocytes. All experiments with *Xenopus* were carried out in accordance with the Swiss federal law on animal welfare, following protocols that had been approved by the committee on animal experimentation of the Canton de Vaud. ASIC currents were measured by two-electrode voltage clamp, and VCF experiments were carried out as described previously (ref. 33; Table S3), with the exception that a different measuring chamber, allowing measurement of current and fluorescence from approximately the same oocyte surface, was used for the kinetics experiments. Kinetic models were fitted directly to the measured currents using the Data2Dynamics software (34). Data are presented as mean ± SEM. Individual experimental data points are provided in *Supporting Information*. Detailed material and methods are provided in *SI Materials and Methods*.

ACKNOWLEDGMENTS. We thank Cláudia Igutti Suenaga Lelli for having carried out some of the experiments, and Omar Alijevic, Olivier Poirot, Laurent Schild, Olivier Staub, and Miguel van Bemmelen for their comments on the manuscript; Gustav Akk for the prototype of the recording chamber; and Ruud Hovius for help with the construction of the recording chamber and for many discussions. This work was supported by Swiss National Science Foundation Grant 31003A_153419 (to S.K.) and by the Swiss Foundation for Excellence and Talent in Biomedical Research and the FP 7 European Union Human Brain Project Grant 604102 (to S.B.). Calculations were performed at the sciCORE (https://scicore.unibas.ch/) scientific computing core facility at University of Basel.

1. Yang L, Palmer LG (2014) Ion conduction and selectivity in acid-sensing ion channel 1. *J Gen Physiol* 144(3):245–255.
2. Wemmie JA, Taugher RJ, Kreple CJ (2013) Acid-sensing ion channels in pain and disease. *Nat Rev Neurosci* 14(7):461–471.
3. Kellenberger S, Schild L (2015) International Union of Basic and Clinical Pharmacology. XCI. Structure, function, and pharmacology of acid-sensing ion channels and the epithelial Na^+ channel. *Pharmacol Rev* 67(1):1–35.
4. Bartoi T, Augustinowski K, Polleichtner G, Gründer S, Ulbrich MH (2014) Acid-sensing ion channel (ASIC) 1a/2a heteromers have a flexible 2:1/1:2 stoichiometry. *Proc Natl Acad Sci USA* 111(22):8281–8286.
5. Jasti J, Furukawa H, Gonzales EB, Gouaux E (2007) Structure of acid-sensing ion channel 1 at 1.9 A resolution and low pH. *Nature* 449(7160):316–323.
6. Gonzales EB, Kawate T, Gouaux E (2009) Pore architecture and ion sites in acid-sensing ion channels and P2X receptors. *Nature* 460(7255):599–604.
7. Baconguis I, Gouaux E (2012) Structural plasticity and dynamic selectivity of acid-sensing ion channel-spider toxin complexes. *Nature* 489(7416):400–405.
8. Baconguis I, Bohlen CJ, Goehring A, Julius D, Gouaux E (2014) X-ray structure of acid-sensing ion channel 1-snake toxin complex reveals open state of a $Na^{(+)}$-selective channel. *Cell* 156(4):717–729.
9. Dawson RJ, et al. (2012) Structure of the acid-sensing ion channel 1 in complex with the gating modifier Psalmotoxin 1. *Nat Commun* 3:936.
10. Krauson AJ, Rued AC, Carattino MD (2013) Independent contribution of extracellular proton binding sites to ASIC1a activation. *J Biol Chem* 288(48):34375–34383.
11. Li T, Yang Y, Canessa CM (2009) Interaction of the aromatics Tyr-72/Trp-288 in the interface of the extracellular and transmembrane domains is essential for proton gating of acid-sensing ion channels. *J Biol Chem* 284(7):4689–4694.
12. Liechti LA, et al. (2010) A combined computational and functional approach identifies new residues involved in pH-dependent gating of ASIC1a. *J Biol Chem* 285(21):16315–16329.
13. Paukert M, Chen X, Polleichtner G, Schindelin H, Gründer S (2008) Candidate amino acids involved in H^+ gating of acid-sensing ion channel 1a. *J Biol Chem* 283(1):572–581.
14. Mourier G, et al. (2016) Mambalgin-1 pain-relieving peptide, stepwise solid-phase synthesis, crystal structure, and functional domain for acid-sensing ion channel 1a inhibition. *J Biol Chem* 291(6):2616–2629.
15. Krauson AJ, Carattino MD (2016) The thumb domain mediates acid-sensing ion channel desensitization. *J Biol Chem* 291(21):11407–11419.
16. Kusama N, Harding AM, Benson CJ (2010) Extracellular chloride modulates the desensitization kinetics of acid-sensing ion channel 1a (ASIC1a). *J Biol Chem* 285(23):17425–17431.
17. Posson DJ, Thompson AN, McCoy JG, Nimigean CM (2013) Molecular interactions involved in proton-dependent gating in KcsA potassium channels. *J Gen Physiol* 142(6):613–624.
18. Askwith CC, Benson CJ, Welsh MJ, Snyder PM (2001) DEG/ENaC ion channels involved in sensory transduction are modulated by cold temperature. *Proc Natl Acad Sci USA* 98(11):6459–6463.
19. Marra S, et al. (2016) Non-acidic activation of pain-related Acid-Sensing Ion Channel 3 by lipids. *EMBO J* 35(4):414–428.
20. Yu Y, et al. (2010) A nonproton ligand sensor in the acid-sensing ion channel. *Neuron* 68(1):61–72.
21. Roy S, et al. (2013) Molecular determinants of desensitization in an ENaC/degenerin channel. *FASEB J* 27(12):5034–5045.
22. Pantazis A, Olcese R (2012) Relative transmembrane segment rearrangements during BK channel activation resolved by structurally assigned fluorophore-quencher pairing. *J Gen Physiol* 140(2):207–218.
23. Mannuzzu LM, Moronne MM, Isacoff EY (1996) Direct physical measure of conformational rearrangement underlying potassium channel gating. *Science* 271(5246):213–216.
24. Cha A, Bezanilla F (1997) Characterizing voltage-dependent conformational changes in the Shaker K^+ channel with fluorescence. *Neuron* 19(5):1127–1140.
25. Schroeder CI, et al. (2014) Chemical synthesis, 3D structure, and ASIC binding site of the toxin mambalgin-2. *Angew Chem Int Ed Engl* 53(4):1017–1020.
26. Salinas M, et al. (2014) Binding site and inhibitory mechanism of the mambalgin-2 pain-relieving peptide on acid-sensing ion channel 1a. *J Biol Chem* 289(19):13363–13373.
27. Chen X, Kalbacher H, Gründer S (2005) The tarantula toxin psalmotoxin 1 inhibits acid-sensing ion channel (ASIC) 1a by increasing its apparent H^+ affinity. *J Gen Physiol* 126(1):71–79.
28. Ramaswamy SS, MacLean DM, Gorfe AA, Jayaraman V (2013) Proton-mediated conformational changes in an acid-sensing ion channel. *J Biol Chem* 288(50):35896–35903.
29. Schuhmacher LN, Srivats S, Smith ES (2015) Structural domains underlying the activation of acid-sensing ion channel 2a. *Mol Pharmacol* 87(4):561–571.
30. Smith ES, Zhang X, Cadiou H, McNaughton PA (2007) Proton binding sites involved in the activation of acid-sensing ion channel ASIC2a. *Neurosci Lett* 426(1):12–17.
31. Kashlan OB, Blobner BM, Zuzek Z, Tolino M, Kleyman TR (2015) Na^+ inhibits the epithelial Na^+ channel by binding to a site in an extracellular acidic cleft. *J Biol Chem* 290(1):568–576.
32. Gwiazda K, Bonifacio G, Vullo S, Kellenberger S (2015) Extracellular subunit interactions control transitions between functional states of acid-sensing ion channel 1a. *J Biol Chem* 290(29):17956–17966.
33. Bonifacio G, Lelli CI, Kellenberger S (2014) Protonation controls ASIC1a activity via coordinated movements in multiple domains. *J Gen Physiol* 143(1):105–118.
34. Raue A, et al. (2015) Data2Dynamics: A modeling environment tailored to parameter estimation in dynamical systems. *Bioinformatics* 31(21):3558–3560.
35. Li P, et al. (2010) Site-specific fluorescence reveals distinct structural changes induced in the human rho 1 GABA receptor by inhibitory neurosteroids. *Mol Pharmacol* 77(4):539–546.
36. Hille B (2001) *Ion Channels of Excitable Membranes* (Sinauer Assoc, Sunderland, MA), 3rd Ed.
37. Pettersen EF, et al. (2004) UCSF Chimera—A visualization system for exploratory research and analysis. *J Comput Chem* 25(13):1605–1612.
38. Mukhtasimova N, Lee WY, Wang HL, Sine SM (2009) Detection and trapping of intermediate states priming nicotinic receptor channel opening. *Nature* 459(7245):451–454.
39. Krashia P, Lape R, Lodesani F, Colquhoun D, Sivilotti LG (2011) The long activations of α2 glycine channels can be described by a mechanism with reaction intermediates ("flip") *J Gen Physiol* 137(2):197–216.
40. Raue A, et al. (2013) Lessons learned from quantitative dynamical modeling in systems biology. *PLoS One* 8(9):e74335.